The essential role of hypermutation in rapid adaptation to antibiotic stress

Heer H. Mehta [a], Amy G. Prater [a], Kathryn Beabout [a*], Ryan A. L. Elworth [b], Mark Karavis [c], Henry S. Gibbons [c] and Yousif Shamoo [a#]

[a] Department of Biosciences, Rice University, Houston, TX, USA

[b] Department of Computer Science, Rice University, Houston, TX, USA

[c] US Army Edgewood Chemical Biological Center, MD, USA

Running head: Hypermutation essential for rapid adaptation

#Address correspondence to Yousif Shamoo, shamoo@rice.edu

[*] Present address: Air Force Research Laboratory, Wright-Patterson AFB, Ohio, USA.

Abstract word count: 198

Text word count: 5693

Abstract

A common outcome of antibiotic exposure in patients and *in vitro* is the evolution of a hypermutator phenotype that enables rapid adaptation by pathogens. While hypermutation is a robust mechanism for rapid adaptation, it requires trade-offs between the adaptive mutations and the more common "hitchhiker" mutations that accumulate from the increased mutation rate. Using quantitative experimental evolution, we examined the role of hypermutation in driving adaptation of *Pseudomonas aeruginosa* to colistin. Metagenomic deep sequencing revealed 2,657 mutations at ≥ 5% frequency in 1,197 genes and 761 mutations in 29 end point isolates. By combining genomic information, phylogenetic analyses, and statistical tests, we showed that evolutionary trajectories leading to resistance could be reliably discerned. In addition to known alleles such as *pmrB,* hypermutation allowed identification of additional adaptive alleles with epistatic relationships. Although hypermutation provided a short-term fitness benefit, it was detrimental to overall fitness. Alarmingly, a small fraction of the colistin adapted population remained colistin susceptible and escaped hypermutation. In a clinical population, such cells could play a role in re-establishing infection upon withdrawal of colistin. We present here a framework for evaluating the complex evolutionary trajectories of hypermutators that applies to both current and emerging pathogen populations.

Importance

Bacteria can increase mutation rates in response to stress as an evolutionary strategy to avoid extinction. However, the complex mutational landscape of hypermutators makes it difficult to distinguish truly adaptive mutations from hitchhikers that follow similar evolutionary trajectories. We provide a framework for evaluating the complex evolutionary trajectories of hypermutators that can be applied to both current and emerging pathogen populations. Using

47 *Pseudomonas aeruginosa* evolving to colistin as a model system, we examine the essential role
48 of hypermutation in the evolution of resistance. Additionally, our results highlight the presence
49 of a subset of cells that survive and remain susceptible during colistin exposure which can serve
50 as a reservoir for re-infection upon withdrawal of the drug in clinical infections. This study
51 provides a broad understanding of hypermutation during adaptation and describes a series of
52 analyses that will be useful in identifying adaptive mutations in well annotated and novel
53 bacterial mutator populations.

54 **Introduction**

55 Hypermutation is a phenomenon that is often observed in clinical isolates of pathogenic species
56 (1–3). The opportunistic pathogen, *Pseudomonas aeruginosa* is a common nosocomial pathogen
57 affecting immunocompromised patients, especially those with cystic fibrosis (CF). 30 to 54% of
58 CF patients infected with *P. aeruginosa* are colonized by hypermutator strains that are associated
59 with reduced lung function and chronic infections (4–6). During infection, *P. aeruginosa* also
60 forms persistent and difficult to clear biofilms that are known to exhibit reduced susceptibility to
61 antimicrobials (7, 8). *P. aeruginosa* also exhibits great metabolic and genetic plasticity allowing
62 it to readily acquire resistance to antibiotics (9). Resistance to the drug of last resort, a cationic
63 antimicrobial peptide (CAP) called colistin (Polymyxin E), has been observed and has been
64 associated with hypermutation (10–13).

65 Mutation acquisition during selection is dependent on mutation supply which can be
66 boosted by hypermutation (14, 15). The typical path leading to a hypermutator phenotype is
67 mutations in the DNA repair system including the MutS/MutL class of proteins (14, 16, 17). The
68 increase in mutation supply accelerates the rate at which bacteria become resistant and thus,
69 hypermutators explore the adaptive evolutionary trajectories leading to resistance more rapidly

70 than non-hypermutators. Interestingly, the dramatic increase in mutation rate also means that
71 many non-adaptive mutations accumulate and are carried along as "hitchhikers" that in the long
72 run are likely to decrease the overall fitness of the organisms in non-selective conditions (18,
73 19). Nevertheless, hypermutation provides a swift strategy for cells undergoing stress to acquire
74 adaptive mutations before they go extinct.

75 Experimental evolution is a powerful approach to understanding the genetic and
76 biochemical basis for antibiotic resistance (16, 20–25). In this work, *P. aeruginosa* PAO1 was
77 evolved to colistin as a continuous culture in a bioreactor where the population was constantly
78 maintained at mid-exponential phase in the presence of sub-inhibitory drug concentrations (24).
79 The observation of hypermutation, accompanied by a dramatic increase in mutation rate among
80 the evolving PAO1 population presented both challenges and opportunities for understanding the
81 evolution of colistin resistance. The potential benefits of this complex data set, however, were
82 equally clear. Hypermutation generated an extensive, if not nearly exhaustive survey of the
83 accessible evolutionary trajectories leading to colistin resistance.

84 We used a combination of phylogenetic and statistical approaches to sort through these
85 complex data, discern truly adaptive alleles from hitchhikers and infer not just the major genetic
86 changes associated with colistin resistance but also those alleles that, in combination with the
87 major players were essential to produce the high minimum inhibitory concentrations (MICs)
88 observed in many clinical isolates (12, 26). Our work has benefited strongly from a series of
89 clinical and *in vitro* experimental evolution studies that have identified many of the major
90 contributors to colistin resistance in *P. aeruginosa* (10, 12, 13, 26, 27).

91 Taken together, our work provides a comprehensive survey of the alleles responsible for
92 *P. aeruginosa* resistance to colistin and perhaps, more importantly, a means to examine future

93 hypermutators in less well characterized or emerging pathogens. The increased mutation rate of
94 hypermutators provides a major adaptive advantage to this pathogen during exposure to colistin.
95 This highlights the strength of hypermutation as an adaptive strategy during exposure to stress
96 and the adaptability of *P. aeruginosa* to survive under such conditions, making it a formidable
97 pathogen.
98
99 **Results**
100 **Hypermutator variants of *P. aeruginosa* emerge rapidly after colistin exposure during**
101 **continuous experimental evolution**
102 *P. aeruginosa* PAO1 was evolved to colistin as a continuous culture in a bioreactor using
103 quantitative experimental evolution (24). The starting MIC of colistin for PAO1 was 1-2 mg/l.
104 Over the course of experiment, the PAO1 population was exposed to increasing, but sub-
105 inhibitory, concentrations of colistin to a final concentration of 16 mg/l colistin, which is four
106 times higher than the clinical breakpoint for resistance of *P. aeruginosa* to colistin (MIC $\geq$
107 4mg/l) (28). Genomic DNA from each daily population was prepared for metagenomic deep
108 sequencing. At the end of the experiment, the final population was serially diluted and spread on
109 a non-selective growth medium for the isolation of end point isolates for whole genome
110 sequencing. The end point isolates produced colonies of diverse morphologies (Supplementary
111 file S1) consistent with the selection of a highly polymorphic population within the bioreactor
112 experiments and this was consistent across duplicate experiments. Single colonies isolated from
113 the final populations ranged from being totally susceptible to totally resistant to colistin which is
114 also consistent with a diverse polymorphic population (Fig. S1 (b) and Table S1). 29 end point
115 isolates were selected for whole genome sequencing.

116 Of the 29 sequenced isolates, 25 contained mutations within *mutS,* the gene encoding the
117 DNA mismatch repair enzyme MutS (Fig. 1). Those end point isolates that had acquired *mutS*
118 mutations had from 44 to 92 mutations each while strains without mutations in *mutS* had 5 to 9
119 mutations showing that mutations within *mutS* correlated with increased genetic diversity.
120 Metagenomic deep sequencing of daily populations showed that on day 10 of adaptation during
121 both, runs 1 and 2 (corresponding to 1.75 mg/l colistin in run 1 and 2 mg/l colistin in run 2),
122 mutations were observed readily in *mutS* (Fig. 1). While the majority of the population contained
123 mutations within *mutS*, a fraction of the final population did not become hypermutators (14.6%
124 in run 1 and 7.6% in run2).
125 As expected, the acquisition of the *mutS* mutations was accompanied by a rapid increase
126 in mutation frequency in the total evolving population. As seen in Figure 2, the starting
127 population on day 1 of evolution, in both runs, had a basal level of diversity. Aside from the
128 underlying diversity in the population, what is apparent from Figure 2 is that as soon as *mutS*
129 mutations arose in both the evolving populations (indicated by red stars), the populations started
130 accumulating more mutations that rose to higher frequencies than mutations contributing to the
131 basal diversity in the population. This was accompanied by increased non-susceptibility of the
132 total population to colistin. Interestingly, lineages derived from Run 1 *mutS* with a 1 bp deletion
133 that introduces a premature stop codon at residue 609 and Run 2 *mutS* with a 10 bp deletion that
134 alters the last 16 amino acids both go to extinction, demonstrating that hypermutation, while
135 increasing the probability of finding successful evolutionary trajectories, does not guarantee
136 success. It may also be that the unsuccessful *mutS* mutant lineages may have stronger mutator
137 phenotypes that accumulate deleterious mutations more rapidly leading to a faster decrease in
138 overall fitness compared to the more successful *mutS* mutants in Runs 1 and 2.

139 **Evolutionary relationship of end point isolates highlights the role of secondary mutations in**
140 **resistance**

141 Phylogenetic trees were constructed to identify the linkages of mutations within the end
142 point isolates (Fig. 3). The 29 sequenced end point isolates had cumulatively acquired 761 total
143 mutations affecting 563 genes. It was interesting to note that in both adaptation runs, isolates that
144 did not acquire *mutS* mutations were phylogenetically closely related to the ancestor and had no
145 increase in colistin resistance. The lack of success in achieving high levels of colistin tolerance
146 by the non-hypermutators highlights the higher efficiency of sampling the potential evolutionary
147 trajectories by strains with elevated mutation rates. End point isolates containing *mutS* mutations
148 had undergone considerable divergence, with each branch varying substantially in total number
149 and type of mutations. It was evident that being a hypermutator alone was not sufficient to
150 acquire resistance. Isolates like I1-6 and I1-76 that had $MutS^{L142P}$ were still susceptible (MIC = 2
151 mg/l) and thus while mutations to *mutS* are drivers for adaptation they are not directly
152 responsible for increased colistin resistance.

153 The highest levels of resistance were achieved by end point isolates that emerged from
154 branches containing mutations in the *pmrAB* genes. Previous studies in *P. aeruginosa* have
155 identified the role of PmrAB in resistance to cationic antimicrobial peptides (CAPs) (29, 30). In
156 Figure 3(a), the branch with the initial *pmrB* mutation diverged into several branches leading to
157 end point isolates that varied in MICs from 16 to 128 mg/l. Similarly, in Figure 3(b), different
158 end point isolates diverging from the same *pmrA* or *pmrB* branch had different colistin MICs.
159 This suggested that although mutations in *pmrAB* were required for achieving resistance,
160 additional mutations in resistant end point isolates were playing an essential role in increasing
161 resistance to colistin.

162 **Hypermutation reveals challenges in distinguishing adaptive mutations from hitchhikers**

163 As the final populations of experimental evolution were dominated by cells with mutator
164 phenotypes, classical genetic approaches for the validation of adaptive alleles such as
165 reintroducing the proposed changes into a clean genomic background were effectively
166 impossible (with an average of 60 mutations per hypermutator end point isolate, there were 60!
167 possible combinations of mutations) and required a different approach. While hypermutation
168 introduced a large number of non-adaptive hitchhiker alleles into both the metagenomic and end
169 point isolate genomic data, the extensive mutational saturation offered a methodological path
170 forward. A statistical approach was used to identify potentially adaptive genes based on the
171 concept that if a larger than expected number of mutations in the same gene across various end
172 point isolates from both the runs were identified then those genes were more likely to be adaptive
173 (16). Under the null hypothesis that all mutations were randomly distributed across the genome,
174 11 genes were identified that were mutated more frequently than expected in the end point
175 isolates using the Fisher's Exact Test (Table 1). A total of 563 genes were mutated in the 29
176 sequenced end point isolates. By plotting the number of mutations per gene versus the
177 percentage of end point isolates having a mutation in that gene (Fig. 4), it was observed that
178 some of the statistically significant genes (p value < 0.001) were located on the top right
179 quadrant. The exception to this was *mutS.* Although *mutS* was seen in 25 of the 29 sequenced
180 end point isolates that have a total of 3 unique mutations in this gene, the *mutS* gene itself was
181 sufficiently long (2568 bp) so that it did not meet the p value cut-off of 0.001 for being called
182 significant. If a gene is very long or if a single mutation or small subset of mutations are the only
183 possible adaptive changes in that gene then it may not rise above the required p value according
184 to the Fisher's Exact Test. This highlights a shortcoming of this particular approach and explains

185 why we combine it with other methods (discussed later) to increase the overall success in
186 identifying adaptive alleles.

187 Among the evolving daily populations from both runs, 1,197 genes were mutated and a
188 total of 2657 mutations were identified at ≥ 5% frequency. When this same test was performed
189 on these mutations, 41 genes were identified as significant (Table 2). Among these 41 genes,
190 four were also identified in the Fisher's Exact Test of the end point isolates (*pmrB, PA0011,*
191 *migA* and *pslA*). *pmrA,* which is known to be involved in resistance, was not identified as a
192 significant gene in the end point isolates but was in the daily populations. The power of this test
193 could certainly be increased by having data from multiple evolving populations instead of the 2
194 runs conducted in this work. Taken together however, the cumulative data from the 2 populations
195 and 29 end point isolates provides an extensive list of genes that potentially play a role in colistin
196 resistance.

197 **Identification of additional genes associated with colistin resistance**

198 Previous studies have been conducted to identify genetic changes leading to polymyxin
199 resistance in *P. aeruginosa* (11–13, 26, 27, 30–32). Since resistance has been often associated
200 with hypermutation (12, 13) which leads to accumulation of a large number of non-adaptive,
201 hitchhiker mutations, not all mutations can be implicated in resistance. However, if the same
202 gene is mutated during adaptation to polymyxin in different studies that use different
203 experimental conditions, it is more likely an adaptative allele than a hitchhiker. We identified
204 such genes that were found to be mutated in our study as well as previous studies and arranged
205 them in the following functional groups: two component system, *pmrAB*, lipopolysaccharide
206 modification and biosynthesis genes (*migA, pagL* and *PA5194*), long chain fatty acid CoA-ligase
207 (*fadD2*), outer membrane protein (*opr86*), probable short chain dehydrogenase *(PA4089)* and

208 multidrug efflux transporter (*mexB*). While the role of some of these genes in polymyxin
209 resistance has been validated (for example, *pmrAB*, *opr86, PA5194*, *pagL* and *mexB*), others
210 have not been previously associated with resistance (12, 13, 27, 30, 33, 34). The targets were
211 mapped on the phylogenetic trees (Fig. 3) to visualize the diversity and distribution of mutations
212 among the end point isolates. The adaptive trajectories of these mutations are shown in Figures
213 S3 and S4. Table 1 provides a list of candidates identified as putative players in colistin
214 resistance among end point isolates and Fig. S5 shows their cellular localization.

215 **The number and variety of mutations observed in *pmrB* suggest that only modest changes**
216 **in PmrB function are required for increased colistin resistance**

217 PmrB is the sensor kinase of a two-component system, PmrAB and is involved in sensing
218 cationic antimicrobial peptides (CAPs) (29). It was noteworthy that during the course of
219 adaptation to colistin, 19 independent mutations were detected in *pmrB* using a 5% frequency
220 cut-off for mutation detection. 18 of these mutations were SNPs that led to amino acid
221 modifications affecting all the domains within this protein while one mutation was a 3 bp
222 deletion leading to the loss of amino acid 47 in PmrB. Out of the 19 mutations, three (L167P,
223 L170P and F408L) were observed independently in duplicate experiments and thus, 16 unique
224 mutations were identified in *pmrB.*

225 Figure 5 shows the putative relationship of PmrB based on canonical sensor kinases of
226 two-component systems. From the positions of mutations shown in red in Figure 5 (b), it is clear
227 that every domain of PmrB was a potential target for adaptive mutations in this study. Also
228 identified on this figure are adaptive mutations identified previously in clinical and lab-adapted
229 *P. aeruginosa* strains (indicated in purple and black) highlighting the plasticity of the gene
230 encoding this protein to acquire mutations. The propensity of *pmrB* to accumulate mutations at

231 many locations suggests that modest changes in PmrB function are sufficient to alter the
232 expression of genes in the regulon of this two-component system sensor kinase and confer
233 resistance.

234 **Introduction of *pmrB* mutations in a wild type PAO1 background indicates that other**
235 **mutations are needed to explain the high levels of resistance**

236 Multiple adaptive mutations identified in colistin resistant end point isolates suggested
237 the possibility of clonal interference where multiple beneficial mutations in the population were
238 competing with one another for success in the population (20). Since the role of PmrB in CAP
239 resistance is known, we wanted to determine if specific changes in PmrB were sufficient to
240 explain the very high MICs of some of the bioreactor end point isolates as well as clinical
241 isolates from previous studies (26). Allelic replacement was used to identify the role of
242 individual *pmrB* mutations in resistance by creating point mutations in *pmrB* within a wild type
243 PAO1 background. 5 such constructs were made, each containing one *pmrB* mutation identified
244 in the colistin evolved PAO1 populations from this work (L17P, L18P, D47G, L243R and
245 F408L). These constructs and their respective bioreactor derived end point isolates were tested to
246 compare colistin MICs (Table 3). Three *pmrB* mutations were observed in end point isolates that
247 had been selected for whole genome sequencing – L18P, L243R and F408L. Sanger sequencing
248 was used to identify the sequence of *pmrB* in a few other end point isolates and 2 isolates,
249 labelled as #11 and #17 were selected that had the D47G and L17P mutations in PmrB,
250 respectively. There is no information regarding other mutations in these isolates since whole
251 genomes of these isolates were not sequenced.

252 From Table 3, it is evident that different mutations within *pmrB* contribute to different
253 levels of colistin resistance. While a mutation constructed in the transmembrane domain of

254 PmrB, L18P imparted complete resistance to colistin (MIC 8 mg/l), adjacent mutation L17P did
255 not (MIC 2 mg/l). The mutation L18P first appeared on day 18 of adaptation (Run 1) while L17P
256 was seen only during the final day of adaptation when the population was growing at 16 mg/l
257 colistin (Fig. S4). While early mutations during adaptation are often the most beneficial,
258 additional mutations conferring typically smaller advantages can arise later (35). Appearance of
259 L18P earlier during adaptation provided resistance to members of a population that was still
260 evolving suggesting that it might be a primary mutation. L17P, which appeared later when the
261 population was already growing at a high drug concentration (16 mg/l) was not an early primary
262 mutation but may have played a role in enhancing the level of resistance in a specific genomic
263 background that had achieved initial success (12). Other point mutations in the periplasmic
264 domain (D47G), dimerization and phosphotransferase (L243R) and in the C-terminal ATP
265 binding domains (F408L) all imparted resistance to colistin with the highest MIC at 8 mg/l while
266 their corresponding bioreactor derived end point isolates consistently had acquired higher levels
267 of resistance. This data provides strong evidence for the role of epistasis in high resistance of the
268 bioreactor derived end point isolates.

269 **PAO1 incurs a fitness cost as a trade-off to acquiring colistin non-susceptibility**

270 Growth characteristics of the constructed mutants and bioreactor end point isolates
271 possessing the same mutation shed light on the fitness of the mutants in the presence and absence
272 of colistin (Fig. 6). The growth of the ancestor, PAO1 served as the reference (Fig. 6 (a)). It was
273 clear from our data that higher levels of colistin resistance, that were associated with
274 hypermutation, led to reduced fitness in the isolates.

275 *pmrB* point mutants constructed in a wild type background could resist up to 8 mg/l
276 colistin without undergoing a severe growth defect in the absence of the drug. In comparison,

277 bioreactor isolates with the same *pmrB* mutations that had higher levels of resistance had
278 decreased fitness in the absence of the drug. Bioreactor isolate I1-37 (doubling time = 397±90
279 minutes; MIC >128 mg/l) grew more than two times slower than the point mutant $PmrB^{L18P}$
280 (doubling time = 165±5 minutes; MIC = 8 mg/l) in the absence of colistin (Fig. 6 (d)). Isolate I1-
281 37, that had 59 mutations in addition to $PmrB^{L18P}$ also had an increased lag time (longer by
282 approximately 125 minutes) and lower overall yield but had the ability to survive in the presence
283 of higher levels of colistin. Similarly, bioreactor isolate I2-55 (MIC = 16 mg/l) had a two-fold
284 decrease in growth rate compared to the point mutant $PmrB^{F408L}$ (MIC = 4 mg/l) (Fig. 6 (f)).
285 However, it was capable of achieving nearly the same final cell density as $PmrB^{F408L}$ as well as
286 the ancestor strain (Fig. 6 (a)) suggesting that higher levels of resistance, as seen in I1-37, were
287 associated with greater fitness defects. Although $PmrB^{L17P}$ alone offered no adaptive advantage
288 (Fig. 6 (a)), bioreactor derived isolate #17 that had a very high colistin MIC also had a severe
289 growth defect.

290 The balance between acquisition of resistance and the associated fitness costs was further
291 supported by allelic replacements to produce $PmrB^{D47G}$ and $PmrB^{L243R}$ in the wild type PAO1
292 background. These adaptive mutants were only modestly less fit in terms of growth rate and
293 yield (Fig. 6 (c), (e) and (f)) under non-selective conditions but were able to grow better than
294 wild type PAO1 in the presence of colistin which is also true for their corresponding bioreactor
295 derived end point isolates.

296 Our data suggests that while *P. aeruginosa* acquires myriad mutations to resist colistin,
297 the accumulation of these mutations comes at a fitness cost to the cells and higher levels of
298 resistance are usually accompanied by a more severe growth phenotype in hypermutators. The
299 advantage of mutation supply in a hypermutator is off-set by the fitness defect of the evolved

300 isolates. In spite of the fitness cost, resistance to this drug of last resort in *P. aeruginosa* clinical
301 isolates has been observed (36–38) which underscores the importance of understanding the
302 mechanism of colistin resistance for the design of new strategies that can circumvent this
303 problem.

304 **Discussion**

305 The development of a hypermutator phenotype is a common occurrence in clinical settings and
306 can lead to rapid adaptation to antibiotics (2, 14). Hypermutators increase the mutation supply
307 within the evolving population allowing natural selection to act upon a more genetically diverse
308 population thereby increasing the probability that a successful, e.g. a more antibiotic resistant
309 variant can be found (18). The increased mutation load however comes with a cost to overall
310 fitness as non-adaptive or hitchhiker mutations accumulate within the genomes of the
311 hypermutators (15). As a random mutation is much more likely to be deleterious, the
312 accumulation of these random mutations brings consequences to fitness especially when the
313 selection pressure of the antibiotic is removed. For example, end-point isolates with increased
314 MICs to colistin had substantially decreased growth rates in the absence of colistin (Fig. 6).
315 While an increased mutation rate may be a poor long term evolutionary path for organisms like
316 *P. aeruginosa*, the short-term benefit is clear. Interestingly, in our bioreactor environments that
317 strongly favor the formation of biofilms, susceptible and non-hypermutator cells persisted
318 despite the vessel containing >2 mg/l colistin for two weeks in the case of Run 1 (Fig. 2). We
319 speculate that the biofilms insulate these weaker variants (Supplementary file S1) and can act as
320 a reservoir for re-establishing a more fit population if the colistin were withdrawn. In an infected
321 individual such as a cystic fibrosis patient, such a reservoir could suggest that when the antibiotic
322 is switched, the more fit *P. aeruginosa* strains can re-emerge and conversely that colistin

323 resistant variants could now be a reservoir for re-establishing the colistin resistant population if
324 the patient returned to colistin therapy. Thus, the combination of hypermutation and strong
325 biofilms can lead to the persistent and difficult to treat infections that are a hallmark of *P.*
326 *aeruginosa.*

327 It has been suggested that because of the large number of hitchhiker mutations that
328 succeed in the population under conditions of selection, the signature of selection in the genome
329 is very weak, making it difficult to distinguish driver alleles from passenger mutations (15). We
330 show that it is possible to identify the signature of selection in an adapting hypermutator
331 population using a combination of genomic and statistical approaches. Quantitative experimental
332 evolution provides a ready means to construct the genomic data needed for analysis (13, 16, 19–
333 21). We propose a hierarchy of analyses beginning with the Fisher's Exact Test of both end-
334 point isolates and longitudinal metagenomic data to build and rank a list of candidate genes that
335 are putatively involved in resistance. This method has proven useful in identification of adaptive
336 mutations in previous studies involving hypermutation and weak selection (16, 19). We also
337 construct phylogenetic trees of the end-point isolates that provide further genetic and
338 evolutionary structure to the candidate list. Furthermore, we use the information about the
339 frequencies of these mutations in the daily populations to build parsimonious evolutionary
340 trajectories for the most important drivers for colistin resistance and taken together these
341 trajectories illustrate what we term the "adaptive genome" of *P. aeruginosa* to the selection
342 environment (Fig. 7).

343 Using genetics and phenotypic analysis of growth rates, we establish that epistatic
344 interactions between multiple mutations in the bioreactor derived hypermutator end point isolates
345 are most likely responsible for the observed higher levels of colistin resistance which comes at a

346 fitness cost to the cells in terms of reduced growth rate and overall yield (Fig. 6). Such epistatic
347 interactions between multiple alleles implies that high levels of colistin resistance can be
348 acquired via multiple adaptive routes which in turn result in the formation of a rugged fitness
349 landscape with many local peaks, each representing a local optimum. Hypermutation provides an
350 effective means for the cells to access this landscape during selection.

351 In summary, this work sheds light on multiple features of *P. aeruginosa's* evolvability to
352 the drug of last resort, colistin. While the complexities of hypermutation have hindered progress,
353 it has become increasingly clear that modern next-gen sequencing and experimental evolution
354 provide a path forward to the study of this clinically and conceptually important evolutionary
355 mechanism for adaptation (13, 16, 39). The methodological approaches within this work show
356 that hypermutation can be studied successfully to produce a broad understanding of adaptive
357 evolution in established as well as in future emerging pathogens.

358

359 **Materials and methods**

360 Bacterial strains, plasmids and growth conditions

361 *P. aeruginosa* PAO1 was obtained from American Type Culture Collection (ATCC 15692).
362 Plasmid pEX18Gm was kindly provided by Dr. Herbert Schweizer. PAO1 was routinely grown
363 in Lysogeny Broth (LB: 10 g/l tryptone, 5 g/l yeast extract, 10 g/l sodium chloride) or on LB +
364 15 g/l bacto agar. Growth medium for adaptation of PAO1 to colistin was LBHI (80% LB + 20%
365 brain heart infusion (BHI) medium) supplemented with 2 mM magnesium sulfate and
366 appropriate concentration of colistin. Colistin stock solution was made by dissolving colistin
367 sulfate (DOT Scientific Inc., MI, USA) in water followed by filter sterilization using a 0.22 µm
368 filter. Cation adjusted Mueller Hinton broth (CA-MHB) was used for minimum inhibitory

369 concentration (MIC) testing and growth curves. Gentamicin at 20 mg/l was used for maintenance
370 of pEX18Gm in *Escherichia coli* and 60 mg/l was used for growing PAO1 transformed with the
371 pEX18-*pmrB* plasmids. Strains and plasmids used in this study are listed in Table 4.

372 Evolution of PAO1 to colistin

373 PAO1 was evolved to colistin in a modified turbidostat as described in (24). In duplicate runs, a
374 300 ml PAO1 culture was established in the bioreactor vessel by using a single colony as
375 inoculum. The culture was maintained in mid-exponential growth phase using respiratory CO_2 as
376 a proxy for turbidity to control media flow. After 12 hours of growth, the first sub-inhibitory
377 dose of colistin was added to the vessel (0.5 mg/l). After that, the culture was monitored and the
378 drug concentration was empirically increased. Details of the process are provided in (24). PAO1
379 was able to grow at 18 mg/l colistin after 26 days of evolution during run 1 and at 16 mg/l
380 colistin after 17 days of evolution during run 2.

381 Isolation and characterization of end point isolates

382 The final resistant population of PAO1 was serially diluted and spread on non-selective medium
383 (LBHI + 2mM magnesium sulfate) to isolate individual members of the population. Each colony
384 was called an end point isolate. 88 end point isolates were selected from run 1 and 82 from run 2
385 for further phenotypic characterization. Morphological characteristics were recorded for each
386 isolate which included colony size, shape, color, consistency and appearance when grown in a
387 non-selective liquid medium (Supplementary file S1). Minimum inhibitory concentration (MIC)
388 of colistin was tested using a preliminary broth microdilution assay. A colistin gradient (0 to 128
389 mg/l) was set up in a 96 well polypropylene plate containing 100 µl CA-MHB per well. 1 µl of
390 an overnight culture (grown in LBHI + 2mM magnesium sulfate) for each isolate was used as
391 inoculum. Plates were incubated at 37ºC and visible growth was recorded after 20-24 hours. The

392 lowest colistin concentration showing absence of growth was the MIC. MIC of other antibiotics
393 were also tested for determining cross-sensitivity/cross-resistance to other drugs. Agar dilution
394 MIC assays were performed for this in 100 mm petri dishes containing CA-MH agar with
395 appropriate drug concentration. A 96 pin applicator was used to spot the overnight culture of
396 each isolate on the agar plates. MICs were recorded after 20-24 hours of incubation at 37ºC.
397 Based on the different phenotypic traits, 15 end point isolates from run 1 and 14 from run 2 were
398 selected for whole genome sequencing and mutation identification. Cross sensitivities to other
399 antibiotics were observed in some end point isolates but a correlation of the cross sensitivity to
400 colistin resistance could not be established and hence, this phenotype was not pursued further.
401 Minimum inhibitory concentration assay
402 Broth microdilution MIC tests in biological triplicate were performed for the 29 end point
403 isolates selected for whole genome sequencing using 96 well polypropylene plates. Each well
404 was filled with 100 µl CA-MHB and appropriate concentration of colistin (0-128 mg/l colistin in
405 2-fold increments). Overnight cultures for end point isolates were grown as biological triplicate
406 in LBHI + 2 mM magnesium sulfate. Optical densities of the cultures were adjusted to 0.05 and
407 5 µl of this OD adjusted culture was used to inoculate each well of the plates. Growth was
408 checked visually after 20-24 hours of incubation at 37ºC and MICs were recorded.
409 Whole genome sequencing and analysis
410 DNA isolation and whole genome sequencing was performed as described in (24). Samples from
411 run 1 of adaptation were sequenced at the US Army Edgewood Chemical Biological Center
412 (ECBC, MD, USA) as 100 bp paired end reads and samples from run 2 were sequenced by a
413 commercial facility (Genewiz, NJ, USA) as 150 bp paired end reads. Read trimming of raw
414 Fastq reads was performed using Sickle (40). Trimmed reads were analyzed using Breseq

415 version 0.30.1 (41) to identify genetic variations between ancestor and adaptive populations as
416 well as end point isolates. The genome sequence of the ancestor was obtained from NCBI
417 (AE004091). The ancestor colony used to inoculate the bioreactor during each run was re-
418 sequenced and the APPLY function on Breseq was used to incorporate any differences in the
419 genome of the re-sequenced ancestor strain into the NCBI reference genome before using it for
420 identifying mutations in the evolved strains. The consensus mode was used for identification of
421 mutations in the end point isolates. The polymorphism mode on Breseq was used for the analysis
422 of daily metagenomic populations from the bioreactor using the following command: -p --
423 polymorphism-reject-surrounding-homopolymer-length 5 --polymorphism-reject-indel-
424 homopolymer-length 0 --polymorphism-minimum-coverage-each-strand 6 --polymorphism-
425 frequency-cutoff 0.02. To filter low quality mutations from the daily populations under analysis,
426 two additional quality-filtering steps were added after the Breseq analysis of each daily sample.
427 It was observed that the number of false calls increased substantially for low frequency
428 mutations. Thus, mutations in the daily populations that fell below a threshold of 5% frequency
429 in the population were filtered out. Second, it was found that mutations had been called in
430 several reads that had low Mapping Quality (MQ) scores. Mutations in regions that contained
431 three or more reads having an MQ score less than 100 were also filtered out. Also, reads were
432 manually examined and mutation calls which were characterized by 3 or more mutations
433 clustered within a read at low frequencies and whose occurrence was not consistent with
434 adaptation or hitchhiking were eliminated from further analysis. Dataset S1 contains a list of all
435 mutations and their frequencies on each day of evolution during Runs 1 and 2.
436 <u>Construction of phylogenetic trees</u>

437 The Breseq output for each end point isolate contained a list of mutations in the genome of the
438 end point isolate. The APPLY function on Breseq was used to apply the mutations in the end
439 point isolate onto the PAO1 reference genome to create a genome sequence for each end point
440 isolate. Next, the genome of the reference strain was manually aligned with that of all the end
441 point isolates using the software MEGA7 (42). Phylogenetic trees were constructed for both runs
442 using the maximum parsimony algorithm based on (43) as implemented in MEGA7. These trees
443 were then visualized using the Dendroscope3 software (44).

444 Fisher's Exact Test

445 To perform the Fisher's Exact Test on end point isolates, a list of the total number of mutations
446 occurring in a gene was compiled from the Breseq output file. Gene lengths were obtained from
447 the Pseudomonas Genome Database (45) by mapping the gene name to the gene length. A few
448 genes without matches were manually given gene lengths. With the compiled list containing the
449 number of mutations per gene, the length of the gene, the total number of mutations in all end
450 point isolates or populations and the total length of the PAO1 genome, a Fisher's Exact Test was
451 performed using the fisher.test function in R with a "two sided" alternative hypothesis and a
452 significance threshold of 0.001.

453 Construction of point mutations in PAO1 *pmrB*

454 Point mutants in PAO1 were constructed using the protocol described in (46) with minor
455 modifications. pEX18Gm was used instead of pEX18Tc. Allelic exchange vectors (Table 4)
456 were made using Gibson Assembly® Master Mix (New England BioLabs) with primers listed in
457 Table 4. Mutant *pmrB* alleles were amplified from the respective bioreactor end point isolate
458 containing the mutation. Electroporation of the constructed plasmid into PAO1 was done at room
459 temperature using a 2mm gap electroporation cuvette at 2.2 kV as described previously (46).

460 Electroporated cells were spread on BHI + 60 mg/l gentamicin (Gm) plates and incubated at
461 37ºC for 2-3 days. Gm resistant colonies were colony purified on BHI + Gm60 plates and single
462 colonies were streaked on no salt LB (NSLB) + 15% sucrose plates and incubated at 30ºC for
463 sucrose counterselection. Sucrose resistant colonies were tested for Gm sensitivity and for
464 colonies that were Gm sensitive and sucrose resistant, the *pmrB* gene was amplified and
465 sequenced using Sanger sequencing to determine presence of the point mutation.

466 Growth curves

467 Overnight cultures were prepared in LB broth in biological triplicate. Optical densities were
468 measured and normalized to 0.05. 96 well polypropylene plates were used for growth curves.
469 Each well was filled with 100 µl CA-MHB and a colistin gradient was set up for concentrations
470 ranging from 0 to 64 mg/l. Each well was inoculated with 1 µl of the OD normalized culture and
471 growth was measured in each well using a BioTek Epoch2 microplate reader at 37ºC for 24
472 hours with optical density being measured at 5-minute intervals. The OD of plain CA-MHB
473 (blank reading) was subtracted from the OD of the samples at every time point. Exponential
474 smoothing was applied to each data series to account for the noise in the OD measurements due
475 to clumping and biofilm formation in the wells. The final graph of OD versus time was plotted
476 using the average of 3 biological replicates with standard deviation. Doubling times were
477 calculated in the OD_{600} interval 0.2 - 0.4.

478

479 **Acknowledgements:** We are thankful to Dr. Luay Nakhleh for his assistance with computational
480 analysis and resources. We are thankful to Dr. Herbert Schweizer for kindly providing plasmids
481 for genetically modifying *P. aeruginosa.* We appreciate the advice provided by Weiliang Huang
482 and Dr. Angela Wilks for isolation and identification of mutant *P. aeruginosa* candidates

483 following allelic replacement. We are grateful to Dr. Jeff Barrick for assistance with analysis of
484 metagenomic population data using Breseq.
485 **Funding:** This work is supported by funds from the Defense Threat Reduction Agency
486 (HDTRA1-15-1-0069) to Y. S., the National Institutes of Health fellowship
487 (F31GM108402NIAID) to K. B. and the National Science Foundation (DMS-1547433) to Luay
488 Nakhleh (PI) and R. A. L. E. (trainee). The content of the information does not necessarily
489 reflect the position or the policy of the federal government, and no official endorsement should
490 be inferred.
491 **Competing interest:** The authors declare no competing interest.
492 **Data availability:** Whole genome sequencing data generated during this study are submitted to
493 the Sequence Read Archive (SRA) database under the BioProject Accession number
494 PRJNA486960.
495 **Author contributions:** Y. S. conceived of the idea. H. H. M., A. P. and K. B. conducted the
496 bioreactor adaptation experiments. M. K. and H. S. G. conducted whole genome sequencing for
497 Run 1 of this project. H. H. M. was involved in analyzing the WGS data and in mutation
498 identification. R. A. L. E. performed the phylogenetic and statistical analysis. H. H. M.
499 performed the phenotypic characterization and allelic replacements. H. H. M. and Y. S. wrote the
500 manuscript. All the authors provided critical feedback and contributed to the manuscript.
501 **Materials and correspondence:** Material requests and correspondence should be addressed to
502 Professor Yousif Shamoo (shamoo@rice.edu).
503

504 **References**

505 1. Swings T, Bergh B Van Den, Wuyts S, Oeyen E, Voordeckers K, Verstrepen KJ, Fauvart

506 M, Verstraeten N, Michiels J. 2017. Adaptive tuning of mutation rates allows fast
507 response to lethal stress in *Escherichia coli*. eLife 6:e22939.

508 2. Hall LMC, Henderson-Begg SK. 2006. Hypermutable bacteria isolated from humans – a
509 critical analysis. Microbiology 152:2505–2514.

510 3. Sundin GW, Weigand MR. 2007. The microbiology of mutability. FEMS Microbiol Lett
511 277:11–20.

512 4. Ciofu O, Riis B, Pressler T, Poulsen HE, Høiby N. 2005. Occurrence of Hypermutable
513 *Pseudomonas aeruginosa* in Cystic Fibrosis Patients Is Associated with the Oxidative
514 Stress Caused by Chronic Lung Inflammation. Antimicrob Agents Chemother 49:2276–
515 2282.

516 5. Waine DJ, Honeybourne D, Smith EG, Whitehouse JL, Dowson CG. 2008. Association
517 between hypermutator phenotype, clinical variables, mucoid phenotype, and antimicrobial
518 resistance in *Pseudomonas aeruginosa.* J Clin Microbiol 46:3491–3493.

519 6. Oliver A, Canton R, Campo P, Baquero F, Blazquez J. 2000. High frequency of
520 hypermutable *Pseudomonas aeruginosa* in cystic fibrosis lung infection. Science
521 288:1251–1253.

522 7. Mulcahy LR, Isabella VM, Lewis K. 2014. *Pseudomonas aeruginosa* biofilms in disease.
523 Microb Ecol 68:1–12.

524 8. Flynn KM, Dowell G, Johnson TM, Koestler BJ, Waters CM, Cooper VS. 2016.
525 Evolution of ecological diversity in biofilms of *Pseudomonas aeruginosa* by altered cyclic
526 diguanylate signaling. J Bacteriol 198:2608–2618.

527 9. Rumbaugh KP. 2014. Genomic complexity and plasticity ensure *Pseudomonas* success.
528 FEMS Microbiol Lett 356:141–143.

529 10. Lee JY, Na IY, Park YK, Ko KS. 2014. Genomic variations between colistin-susceptible
530 and -resistant *Pseudomonas aeruginosa* clinical isolates and their effects on colistin
531 resistance. J Antimicrob Chemother 69:1248–1256.

532 11. Abraham N, Kwon DH. 2009. A single amino acid substitution in PmrB is associated with
533 polymyxin B resistance in clinical isolate of *Pseudomonas aeruginosa*. FEMS Microbiol
534 Lett 298:249–254.

535 12. Jochumsen N, Marvig RL, Damkiær S, Jensen RL, Paulander W, Molin S, Jelsbak L,
536 Folkesson A. 2016. The evolution of antimicrobial peptide resistance in *Pseudomonas*
537 *aeruginosa* is shaped by strong epistatic interactions. Nat Commun 7:13002.

538 13. Dobelmann B, Willmann M, Steglich M, Bunk B, Nubel U, Peter S, Neher RA. 2017.
539 Rapid and consistent evolution of colistin resistance in extensively drug-resistant
540 *Pseudomonas aeruginosa* during morbidostat culture. Antimicrob Agents Chemother
541 61:e00043-17.

542 14. Denamur E, Matic I. 2006. Evolution of mutation rates in bacteria. Mol Microbiol
543 60:820–827.

544 15. Couce A, Caudwell L V., Feinauer C, Hindré T, Feugeas J, Weigt M, Lenski RE,
545 Schneider D, Tenaillon O. 2017. Mutator genomes decay , despite sustained fitness gains ,
546 in a long-term experiment with bacteria. Proc Natl Acad Sci 114:9026–9035.

547 16. Hammerstrom TG, Beabout K, Clements TP, Saxer G, Shamoo Y. 2015. *Acinetobacter*

548 *baumannii* repeatedly evolves a hypermutator phenotype in response to tigecycline that
549 effectively surveys evolutionary trajectories to resistance. PLoS One 10:e0140489.

550 17. Dettman JR, Sztepanacz JL, Kassen R. 2016. The properties of spontaneous mutations in
551 the opportunistic pathogen *Pseudomonas aeruginosa*. BMC Genomics 17:27.

552 18. Tenaillon O, Taddei F, Radman M, Matic I. 2001. Second-order selection in bacterial
553 evolution : selection acting on mutation and recombination rates in the course of
554 adaptation. Res Microbiol 152:11–16.

555 19. Saxer G, Krepps MD, Merkley ED, Ansong C, Kaiser BLD, Valovska M-T, Ristic N, Yeh
556 PT, Prakash VP, Leiser OP, Nakhleh L, Gibbons HS, Kreuzer HW, Shamoo Y. 2014.
557 Mutations in global regulators lead to metabolic selection during adaptation to complex
558 environments. PLOS Genet 10:e1004872.

559 20. Cooper VS. 2018. Experimental evolution as a high-throughput screen for genetic
560 adaptations. mSphere 3:e00121-18.

561 21. Miller C, Kong J, Tran TT, Arias CA, Saxer G, Shamoo Y. 2013. Adaptation of
562 *Enterococcus faecalis* to daptomycin reveals an ordered progression to resistance.
563 Antimicrob Agents Chemother 57:5373–5383.

564 22. Beabout K, Hammerstrom TG, Wang TT, Bhatty M, Christie PJ, Saxer G, Shamoo Y.
565 2015. Rampant parasexuality evolves in a hospital pathogen during antibiotic selection.
566 Mol Biol Evol 32:2585–97.

567 23. Mehta H, Weng J, Prater A, Elworth RAL, Han X, Shamoo Y. 2018. Pathogenic *Nocardia*
568 *cyriacigeorgica* and *Nocardia nova* evolve to resist trimethoprim- sulfamethoxazole by

569 both expected and unexpected pathways. Antimicrob Agents Chemother AAC.00364-18.

570 24. Mehta HH, Prater AG, Shamoo Y. 2018. Using experimental evolution to identify
571 druggable targets that could inhibit the evolution of antimicrobial resistance. J Antibiot
572 (Tokyo) 71:279–286.

573 25. Toprak E, Veres A, Michel J-B, Chait R, Hartl DL, Kishony R. 2012. Evolutionary paths
574 to antibiotic resistance under dynamically sustained drug selection. Nat Genet 44:101–
575 105.

576 26. Moskowitz SM, Brannon MK, Dasgupta N, Pier M, Sgambati N, Miller AK, Selgrade SE,
577 Miller SI, Denton M, Conway SP, Johansen HK, Høiby N. 2012. PmrB mutations
578 promote polymyxin resistance of *Pseudomonas aeruginosa* isolated from colistin-treated
579 cystic fibrosis patients. Antimicrob Agents Chemother 56:1019–1030.

580 27. Lee JY, Park YK, Chung ES, Na IY, Ko KS. 2016. Evolved resistance to colistin and its
581 loss due to genetic reversion in *Pseudomonas aeruginosa.* Sci Rep 6:25543.

582 28. Clinical and Laboratory Standards Institute (CLSI). 2017. Performance Standards for
583 Antimicrobial Susceptibility Testing; 27th Ed. CLSI supplement M100.

584 29. McPhee JB, Lewenza S, Hancock REW. 2003. Cationic antimicrobial peptides activate a
585 two-component regulatory system, PmrA-PmrB, that regulates resistance to polymyxin B
586 and cationic antimicrobial peptides in *Pseudomonas aeruginosa.* Mol Microbiol 50:205–
587 217.

588 30. Moskowitz SM, Ernst RK, Miller SI. 2004. PmrAB, a Two-Component Regulatory
589 System of *Pseudomonas aeruginosa* that modulates resistance to cationic antimicrobial

590 peptides and addition of aminoarabinose to lipid A. J Bacteriol 186:575–579.

591 31. Lee JY, Ko KS. 2014. Mutations and expression of PmrAB and PhoPQ related with
592 colistin resistance in *Pseudomonas aeruginosa* clinical isolates. Diagn Microbiol Infect
593 Dis 78:271–276.

594 32. Barrow K, Kwon DH. 2009. Alterations in two-component regulatory systems of *phoPQ*
595 and *pmrAB* are associated with polymyxin B resistance in clinical isolates of
596 *Pseudomonas aeruginosa.* Antimicrob Agents Chemother 53:5150–5154.

597 33. Pamp SJ, Gjermansen M, Johansen HK, Tolker-Nielsen T. 2008. Tolerance to the
598 antimicrobial peptide colistin in *Pseudomonas aeruginosa* biofilms is linked to
599 metabolically active cells , and depends on the *pmr* and *mexAB-oprM* genes. Mol
600 Microbiol 68:223–240.

601 34. Han M, Velkov T, Zhu Y, Roberts KD, Brun AP Le, Chow SH, Gutu AD, Moskowitz
602 SM, Shen H, Li J. 2018. Polymyxin-Induced Lipid A Deacylation in *Pseudomonas*
603 *aeruginosa* Perturbs Polymyxin Penetration and Confers High-Level Resistance. ACS
604 Chem Biol 13:121–130.

605 35. Barrick JE, Yu DS, Yoon SH, Jeong H, Oh TK, Schneider D, Lenski RE, Kim JF. 2009.
606 Genome evolution and adaptation in a long-term experiment with *Escherichia coli*. Nature
607 461:1243–1247.

608 36. Oliveira dos Santos S, Martins La Rocca S, Hörner R. 2016. Colistin resistance in non-
609 fermenting Gram-negative bacilli in a university hospital. Brazilian J Infect Dis 20:649–
610 650.

611 37. Ramesh N, Prasanth M, Ramkumar S, Suresh M, Tamhankar AJ, K.M. G, Karthikeyan S,
612 Bozdogan B. 2016. Colistin susceptibility of gram-negative clinical isolates from Tamil
613 Nadu , India. Asian Biomed 10:35–39.

614 38. Denton M, Kerr K, Mooney L, Keer V, Rajgopal A, Brownlee K, Arundel P, Conway S.
615 2002. Transmission of colistin-resistant *Pseudomonas aeruginosa* between patients
616 attending a pediatric cystic fibrosis center. Pediatr Pulmonol 34:257–261.

617 39. Swings T, Weytjens B, Schalck T, Bonte C, Verstraeten N, Michiels J, Marchal K. 2017.
618 Network-Based Identification of Adaptive Pathways in Evolved Ethanol-Tolerant
619 Bacterial Populations. Mol Biol Evol 34:2927–2943.

620 40. Joshi NA, Fass JN. 2011. Sickle: A sliding-window, adaptive, quality-based trimming tool
621 for FastQ files (Version 1.33) [Software]. Available at https://github.com/najoshi/sickle.

622 41. Deatherage DE, Barrick JE. 2014. Identification of mutations in laboratory evolved
623 microbes from next-generation sequencing data using breseq. Methods Mol Biol
624 1151:165–188.

625 42. Kumar S, Stecher G, Tamura K. 2016. MEGA7 : Molecular Evolutionary Genetics
626 Analysis version 7 . 0 for bigger datasets. Mol Biol Evol 33:1870–1874.

627 43. Nei M, Kumar S. 2000. Molecular evolution and phylogenetics. Oxford University Press,
628 Oxford.

629 44. Huson DH, Scornavacca C. 2012. Dendroscope 3 : An interactive tool for rooted
630 phylogenetic trees and networks. Syst Biol 61:1061–1067.

631 45. Winsor GL, Griffiths EJ, Lo R, Dhillon BK, Shay JA, Brinkman FSL. 2016. Enhanced

632 annotations and features for comparing thousands of *Pseudomonas* genomes in the
633 Pseudomonas genome database. Nucelis Acids Res 44:646–653.

634 46. Huang W, Wilks A. 2017. A rapid seamless method for gene knockout in *Pseudomonas*
635 *aeruginosa*. BMC Microbiol 17:199.

636 47. Bhate MP, Molnar KS, Goulian M, DeGrado WF. 2015. Signal Transduction in Histidine
637 Kinases: Insights from New Structures. Structure 23:981–994.

638 48. Schurek KN, Sampaio JLM, Kiffer CR V, Sinto S, Mendes CMF, Hancock REW. 2009.
639 Involvement of *pmrAB* and *phoPQ* in Polymyxin B Adaptation and Inducible Resistance
640 in Non-Cystic Fibrosis Clinical Isolates of *Pseudomonas aeruginosa*. Antimicrob Agents
641 Chemother 53:4345–4351.

642 49. Poon KKH, Westman EL, Vinogradov E, Jin S, Lam JS. 2008. Functional characterization
643 of MigA and WapR : Putative rhamnosyltransferases involved in outer core
644 oligosaccharide biosynthesis of *Pseudomonas aeruginosa*. J Bacteriol 190:1857–1865.

645 50. Billings N, Millan MR, Caldara M, Rusconi R, Tarasova Y, Stocker R, Ribbeck K. 2013.
646 The extracellular matrix component Psl provides fast- acting antibiotic defense in
647 *Pseudomonas aeruginosa* biofilms. PLoS Pathog 9:e1003526.

648 51. Lee J, Chung ES, Na IY, Kim H, Shin D, Ko KS. 2014. Development of colistin
649 resistance in *pmrA-, phoP-, parR-* and *cprR*-inactivated mutants of *Pseudomonas*
650 *aeruginosa*. J Antimicrob Chemother 69:2966–2971.

651 52. Hoang TT, Karkhoff-Schweizer RR, Kutchma AJ, Schweizer HP. 1998. A broad-host-
652 range Flp- FRT recombination system for site-specific excision of chromosomally-located

653 DNA sequences : application for isolation of unmarked *Pseudomonas aeruginosa* mutants.
654 Gene 212:77–86.

655

656

657 **Figure legends**

658 **Figure 1**. *mutS* mutations observed during adaptation of *P. aeruginosa* populations to colistin. In
659 duplicate experiments (Run 1 and Run 2), mutations were seen in the *mutS* gene. The specific
660 mutations identified, their effect on MutS and their abundance in the evolved populations are
661 indicated (mutation detection cut-off = 5%). The last column shows the frequency for each *mutS*
662 mutation over the course of evolution. The X-axis shows the day of adaptation (26 days in Run 1
663 and 17 in Run 2) and the Y-axis indicates the percentage of the total population that possessed
664 the mutation.

665 **Figure 2**. Single nucleotide polymorphism (SNP) map of the PAO1 populations evolving to
666 colistin (Run 1 and Run 2). For ease of comparison, the graphs represent a linearized genome of
667 PAO1 with SNP positions indicated on the X-axis. The X-axis is not distributed evenly but
668 denotes positions on the genome carrying mutations. This is done to highlight regions of the
669 genome with higher mutation density. The Y-axis is the frequency of the mutation in the total
670 population. For each run of adaptation, graphs of daily sampled populations are stacked (26 days
671 of evolution for Run 1 and 17 days for Run 2). Red stars indicate days on which *mutS* mutations
672 arose in each population. The color gradient on the right side of each panel shows the step-wise
673 increase in colistin concentration experienced by the populations during adaptation. The
674 increased genetic diversity in the region from 7.8×10^5 to 8×10^5 bp on the PAO1 genome can be

675 attributed to the Pf4 phage island (indicated by asterisk), details of which are provided in
676 Supplementary file S1.
677 **Figure 3**. Phylogenetic trees for end point isolates obtained from experimental evolution Runs 1
678 (a) and 2 (b). PAO1: Ancestor. Isolate names are at the right side of each branch. Orange text
679 following the isolate name denotes its colistin MIC and in parenthesis are the total number of
680 mutations identified in that particular isolate. Branches with mutations in putative targets
681 identified in this study have names of mutated genes on them. Targets in purple text were
682 identified by the Fisher's Exact test of end point isolates and targets underlined were common
683 among our study and other polymyxin resistance studies. *mutS* mutations are identified in red
684 text. The large number of mutations per hypermutator lineage precludes their complete inclusion
685 in these phylogenetic trees. The complete list of mutations in each end point isolate can be found
686 in Dataset S1.
687 **Figure 4**. Genes mutated more frequently than expected identified using Fisher's Exact Test.
688 Number of mutations identified within a single gene among the 29 sequenced end point isolates
689 was plotted against the percentage of end point isolates containing a mutation in that gene. Genes
690 identified as significant with a *p* value less than 0.001 in the Fisher's Exact Test are highlighted
691 in red. False noise has been added to the data points to separate them on the graph. Detailed
692 analysis of this graph is provided in Supplementary file S1.
693 **Figure 5**: (a) Structural representation of a canonical two-component system sensor kinase dimer
694 (adapted from (47)) and (b) linear map of *pmrB* showing positions of identified mutations. The
695 color scheme for domains used in (a) has been maintained in (b). Mutations identified in *pmrB* in
696 this study as well as previous works have been indicated by vertical lines on the *pmrB* gene (b).
697 Red lines represent mutations identified in this study. Black lines represent mutations observed

698 in other evolution experiments (12, 13, 27, 30) and purple lines represent mutations identified in
699 colistin resistant clinical *P. aeruginosa* isolates (10–12, 26, 31, 32, 48). HAMP: histidine
700 kinases, adenylate cyclases, methyltransferases and phosphodiesterases; DHP: dimerization and
701 histidine phosphotransfer. Domain assignments in the PmrB protein are based on the predicted
702 domain structure of PmrB of Moskowitz et al. (26). Details of the types of mutations observed in
703 each domain of PmrB in this study can be found in Supplementary file S1.
704 **Figure 6**. Growth characteristics of PAO1 ancestor, constructed point mutants and bioreactor
705 adapted end point isolates. Each panel (except (a)) represents the constructed mutant on the left
706 and the bioreactor adapted end point isolate carrying the same *pmrB* mutation on the right. All
707 growth assays were conducted at colistin concentrations ranging from 0 to 64 mg/l. Error bars
708 represent the standard deviation of three biological replicates. MICs of all these strains,
709 measured by broth microdilution, are on the top right corner of each graph.
710 **Figure 7.** Adaptive genome of a *P. aeruginosa* population (Run 1) evolving to colistin. Most
711 adaptive genes had multiple mutations within them during the course of adaptation. On a given
712 day, the sum of frequencies of the different alleles within a gene was calculated and plotted on
713 the Y-axis. The X-axis represents the day of adaptation and the Z-axis represents each gene.
714 Genes represented here include putative candidates listed in Table 1 and selected candidates
715 from Table 2 (selection based on their appearance in other polymyxin resistance studies).
716
717
718
719
720

721 Table 1. Putative targets involved in colistin resistance in PAO1 based on mutations observed in

722 end point isolates

723

Gene name	Mutation(s) identified in end point isolates	*p*-value from Fisher's Exact Test	Function
Fisher's Exact Test of end point isolates			
migA	frameshifts, V170M, H219P	5.58e-6	Alpha-1,6-rhamnosyl transferase, responsible for uncapped core oligosaccharides in the LPS (49)
mvfR	Y77H, V162A, L6P, V9V	8.39e-6	Quorum sensing and virulence regulator
pmrB	L18P, G348S, L243R, F408L	3.4e-5	Two component system involved in cationic antimicrobial sensing and resistance (30)
pslA	frameshifts, 700 bp deletion, G364D, R229C, Y268H	3.43e-5	Exopolysaccharide involved in biofilm formation; involved in biofilm resistance to antibiotics (50)
yfiR	L183P, C71S, Y58C	5.43e-5	Part of c-di-GMP regulator system involved in biofilm formation.
lasR	L118P, G235D, T115A	1.06e-4	Quorum sensing regulator
PA5194	W64*, G227D, W239*	1.46e-4	LpxT; phosphorylation of lipid A
PA0011	frameshifts, W33*	1.96e-4	2-hydroxylauroyl transferase; transfers 2-hydroxylaurate to C-2 position of lipid A
gltS	A194V, G351S, L126L	4.86e-4	Glutamate/sodium symporter
PA4900	L321P, P339P, Q4*	6.45e-4	Probable major facilitator superfamily transporter
PA0494	A44V, P56L, Y201Y	6.96e-4	Probable acyl-CoA carboxylase subunit
Observed in other polymyxin resistance studies of *P. aeruginosa*			
pmrAB	G19E, L18P, G348S, L243R, F408L		Two component system involved in cationic antimicrobial sensing and resistance (12, 13, 27, 30)
migA	frameshifts, V170M, H219P		Alpha-1,6-rhamnosyl transferase, responsible for uncapped core oligosaccharides in the LPS (12, 13)
PA5194	W64*, G227D, W239*		Lipid a kinase; adds phosphate group to lipid A (12)
fadD2	Q245R		Long chain fatty acid CoA ligase (12)
opr86	D535N		Outer membrane protein (12)
PA4089	G105D		Probable short chain dehydrogenase involved in fatty acid biosynthesis (27)
pagL	D118G		Lipid A deacylation, upregulated by polymyxin (34)
mexB	T242A, T295A		RND multidrug efflux transporter (12)

724

725

726

727 Table 2: Candidate colistin resistance genes identified as significant by Fisher's Exact Test of

728 daily populations

Gene	Number of mutation events	Function	*p*-value	Comments
LPS modification				
pmrB	19	Pmrb: two-component regulator system signal sensor kinase pmrb	4.41E-22	Also identified in Fisher's Exact Test of end point isolates
PA0011	9	Probable 2-OH-lauroyltransferase	3.19E-10	Also identified in Fisher's Exact Test of end point isolates
migA	8	Alpha-1,6-rhamnosyltransferase	8.37E-09	Also identified in Fisher's Exact Test of end point isolates
pmrA	4	Two-component regulator system response regulator pmra	2.15E-04	Involved in polymyxin resistance (51)
Biofilm synthesis				
pelA	13	Modification and secretion system for PEL polysaccharide dependent biofilm	6.44E-10	Mutations in PEL polysaccharide genes also identified in (10, 12)
pslA	8	Psl polysaccharide synthesis and biofilm formation	2.85E-07	Also identified in Fisher's Exact Test of end point isolates
algP	7	Alginate regulatory protein	5.11E-07	
pslN	4	Involved in Psl biosynthesis	9.81E-04	Part of operon containing *pslA*
Unknown role				
wspA	9	Probable chemotaxis transducer	5.53E-08	
PA1336	8	Probable two-component sensor	2.24E-06	
PA3272	11	Probable ATP-dependent DNA helicase	4.02E-06	Mutation in PA3272 also identified in (12)
ostA	9	Organic solvent tolerance protein	4.28E-06	
vfr	5	Transcriptional regulator	1.04E-05	
PA4133	6	Cytochrome c oxidase subunit (cbb3 type)	4.17E-05	
PA4021	6	Probable transcriptional regulator	2.13E-04	
PA4873	5	Probable heat-shock protein	2.42E-04	
pqqD	3	Pyrroloquinoline quinone biosynthesis protein D	2.58E-04	
exbB1	4	Transport protein exbb	2.89E-04	
PA2802	4	Probable transcriptional regulator	2.89E-04	
ureD	4	Urease accessory protein	5.19E-04	
pqqF	6	Pyrroloquinoline quinone biosynthesis protein F	5.64E-04	
hitB	5	Iron (III)-transport system permease	5.83E-04	
PA0181	4	Probable transcriptional regulator	7.55E-04	

PA4180	5	Probable acetolactate synthase large subunit	7.82E-04	
PA3900	4	Probable transmembrane sensor	8.20E-04	
PA0041	13	Probable hemagglutinin	8.20E-04	
PA2511	4	Probable transcriptional regulator	9.81E-04	

729 NOTE: Genes within the Pf4 phage encoded region identified by this test were excluded from this table.
730 Genes encoding hypothetical proteins identfied by this test are listed in Table S2.
731

732

733 Table 3. Comparison of constructed *pmrB* mutants and bioreactor derived end point isolates

734 having the same *pmrB* mutation

Mutation	**Colistin MIC (mg/l) of constructed mutant**	**Colistin MIC (mg/l) of end point isolates with this mutation**	**Frequency of mutation at the end of adaptation (run1 and run 2)**	**Number of additional mutations in end point isolates having this mutation**
WT	1/2	-	-	
L17P	2	>128	46%	Not determined[b]
L18P	8	16 to 128 [a]	10%	53 to 62
D47G	8	16	4.3%	Not determined[b]
L243R	4	16 to 32 [a]	5.1%	60 to 74
F408L	4	8 to 64 [a]	3.6% and 22.8%	56 to 68

735 MIC: Minimal inhibitory concentration
736 a Shows range of MICs for different end point isolates with this mutation
737 b Whole genome sequencing for these end point isolates was not performed
738

739

740 Table 4. Bacterial strains, plasmids and primers used in this study.

Strain/plasmid	**Characteristics**	**Source**
Strains		
PAO1	*Pseudomonas aeruginosa* ancestor	ATCC 15692
NEB 5-alpha	*Escherichia coli* DH5α derivative	New England Biolabs C2987I
PAO1- $PmrB^{F408L}$	Point mutant PAO1 *pmrB*$^{1222T->C}$ encoding $PmrB^{F408L}$	This study

PAO1- PmrB^{D47G}	Point mutant PAO1 *pmrB*$^{140A->G}$ encoding PmrB^{D47G}	This study
PAO1- PmrB^{L243R}	Point mutant PAO1 *pmrB*$^{728T->G}$ encoding PmrB^{L243R}	This study
PAO1-PmrB^{L18P}	Point mutant PAO1 *pmrB*$^{53T->C}$ encoding PmrB^{L18P}	This study
PAO1- PmrB^{L17P}	Point mutant PAO1 *pmrB*$^{50T->C}$ encoding PmrB^{L17P}	This study
Plasmids		
pEX18Gm	Gm^{R}; *oriT*$^{+}$ *sacB*$^{+}$, gene replacement vector with MCS from pUC18	(52)
pEX18Gm-*pmrB*$^{1222T->C}$	*pmrB*$^{1222T->C}$ allelic exchange vector for mutant encoding PmrB^{F408L}	This study
pEX18Gm-*pmrB*$^{140A->G}$	*pmrB*$^{140A->G}$ allelic exchange vector for mutant encoding PmrB^{D47G}	This study
pEX18Gm-*pmrB*$^{728T->G}$	*pmrB*$^{728T->G}$ allelic exchange vector for mutant encoding PmrB^{L243R}	This study
pEX18Gm-*pmrB*$^{53T->C}$	*pmrB*$^{53T->C}$ allelic exchange vector for mutant encoding PmrB^{L18P}	This study
pEX18Gm-*pmrB*$^{50T->C}$	*pmrB*$^{50T->C}$ allelic exchange vector for mutant encoding PmrB^{L17P}	This study
Primer	**Sequence**	**Template**
1. Cloning *pmrB*^{F408L} into pEX18Gm		
F408L-500F	ctgcaaggcgattaagttggCTCATCGACGAACTCAACCT	I2-55
F408L-500R	gattacgaattcgagctcggCTCCTCGATCTTGCGATTCA	
pEX-F408L-500F	TGAATCGCAAGATCGAGGAGccgagctcgaattcgtaatc	pEX18Gm
pEX-F408L-500R	AGGTTGAGTTCGTCGATGAGccaacttaatcgccttgcag	
2. Cloning *pmrB*^{D47G} into pEX18Gm		
pmrB-D47G-fwd	ctgcaaggcgattaagttggTGACCAAGCCCTTCGATCTCG	colony #11
pmrB-D47G-rev	gattacgaattcgagctcggGCGGATCTCCAGCGGTACCG	
pEX-D47G-fwd	CGGTACCGCTGGAGATCCGCccgagctcgaattcgtaatc	pEX18Gm
pEX-D47G-rev	GAGATCGAAGGGCTTGGTCAccaacttaatcgccttgcag	

3. Cloning *pmrB*^{L243R} into pEX18Gm		
pmrB-L243R-fwd	ctgcaaggcgattaagttggGACCTTGCCACCGAAGACCA	I2-58
pmrB-L243R-rev	gattacgaattcgagctcggGTAGAAGCGGGTGAAGATCG	
pEX-L243R-fwd	CGATCTTCACCCGCTTCTACccgagctcgaattcgtaatc	pEX18Gm
pEX-L243R-rev	TGGTCTTCGGTGGCAAGGTCccaacttaatcgccttgcag	
4. Cloning *pmrB*^{L18P} into pEX18Gm		
L18P-450F	tgtgctgcaaggcgattaagCCGACGACTACCTGACCAAG	I1-58
L18P-450R	ggtacccggggatcctctagGTAGAACAGCAGCAGGTTCA	
pEX-L18P-450F	TGAACCTGCTGCTGTTCTACctagaggatccccgggtacc	pEX18Gm
pEX-L18P-450R	CTTGGTCAGGTAGTCGTCGGcttaatcgccttgcagcaca	
5. Cloning *pmrB*^{L17P} into pEX18Gm		
L18P-450F	tgtgctgcaaggcgattaagCCGACGACTACCTGACCAAG	colony #17
L18P-450R	ggtacccggggatcctctagGTAGAACAGCAGCAGGTTCA	
pEX-L18P-450F	TGAACCTGCTGCTGTTCTACctagaggatccccgggtacc	pEX18Gm
pEX-L18P-450R	CTTGGTCAGGTAGTCGTCGGcttaatcgccttgcagcaca	

741

742 **Supplemental material legends**

743 **Figure S1**. Phenotypic diversity of end point isolates obtained at the end of adaptation of PAO1
744 to colistin. (a) End point isolates showed variations in the size, color and texture. (b) Pie chart
745 showing colistin minimum inhibitory concentrations (MICs) of end point isolates. Numbers in
746 each segment represent the actual number of isolates from that population having the specific

747 colistin MIC as indicated by the colors in the legend. 12 out of 88 isolates from run 1 (14%) and
748 19 out of the 82 isolates from run 2 (23%) were colistin susceptible (MIC $\leq$ 2 mg/l).
749 **Figure S2**. (a) Excision and circularization of phage Pf4 upon colistin exposure. The prophage,
750 Pf4 exists in lysogenic state in PAO1. During exposure to colistin, the phage encoded DNA
751 excised from the PAO1 chromosome and formed superinfective phage. (b) Induction of
752 prophage during evolution of PAO1 to colistin. Top left panel shows different dilutions of the
753 supernatant from day 1 of evolution (before drug exposure) that are incapable of lysing the lawn
754 of PAO1 on the plate. The supernatant obtained after centrifugation of the population sample
755 was filter sterilized and then serially diluted (10-fold dilutions) in SM buffer (50 mM Tris-HCl,
756 pH 7.5 + 100 mM NaCl + 10 mM $MgSO_4.7H_2O$). 5 µl of each dilution was spotted on a lawn of
757 PAO1. Supernatant from day 2 (first instance of drug exposure) has strong lytic activity (top
758 right) suggesting induction of prophage and lytic capability. This lytic capability continues to
759 exist till the end of adaptation (bottom panels -days 13 and 25). All these samples are from run 1
760 of adaptation that lasted 26 days.
761 **Figure S3**. Evolutionary trajectories of adaptive mutations identified in this study. Each graph is
762 a plot of the frequency of a mutation in a gene within the population versus the day of adaptation
763 on which it was observed. Multiple mutations within a gene are plotted on the same graph using
764 different colors to represent each mutation. Only alleles that rose above 10% frequency during
765 adaptation are shown here. Evolutionary trajectories of the adaptive alleles of *pmrB* are shown in
766 Figure S4.
767 **Figure S4**. Trajectories of *pmrB* mutations detected at $\geq$ 5% frequency during adaptation to
768 colistin. 11 mutations were identified in run 1 which lasted 26 days. Out of the 11, only 3
769 mutations, L17P, L18P and L167P were detected in the final resistant population at $\geq$ 5%

770 frequency. Run 2 which lasted 17 days had 8 *pmrB* mutations in the evolving population with
771 only 2 mutations, L243R and F408L detectable in the final resistant population.
772 **Figure S5**. Cellular localization of targets identified in this study playing putative roles in
773 colistin resistance. Targets in purple text were identified by the Fisher's Exact test of end point
774 isolates and targets underlined were common among our study and other polymyxin resistance
775 studies.
776 **Figure S6**. Relationship between colistin MIC of an end point isolate and its biofilm forming
777 capability as measured by crystal violet staining. No significant co-relation between level of
778 resistance of the isolate and its biofilm forming capability can be inferred from this data.
779 **Table S1.** List of end point isolates selected for whole genome sequencing and their minimum
780 inhibitory concentrations (MICs) to colistin
781 **Table S2**. Hypothetical protein encoding genes identified as significant by Fisher's Exact Test
782 performed on mutations in daily populations of PAO1 evolving to colistin
783 **Dataset S1.** Mutations identified in daily populations and well as in end point isolates obtained
784 from adaptation of PAO1 to colistin during Run 1 and Run 2.

Mutation in *mutS*	Effect of mutation	Frequency on final day of adaptation	Mutational trajectory
<u>Run1:</u>			
L142P	Point mutation in connector domain of MutS	78.7%	
1bp deletion at nucleotide position 1745	Premature stop codon at amino acid position 609 (Wild type MutS=855 amino acids)	6.7%	
<u>Run2:</u>			
9 bp deletion (nucleotides 1536 to 1544)	Deletion of amino acids 512-514 in the lever domain of MutS	92.4%	
10 bp deletion (nucleotides 2520 to 2529)	Extends open reading frame and alters last 16 amino acids of MutS	0%	

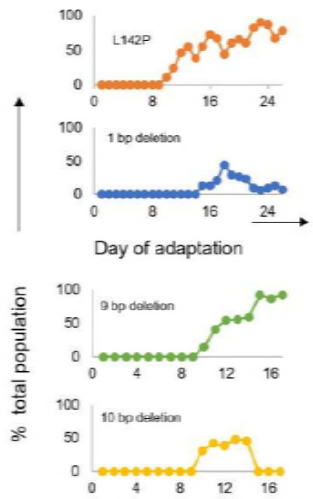

Figure 1. *mutS* mutations observed during adaptation of *P. aeruginosa* populations to colistin. In duplicate experiments (Run 1 and Run 2), mutations were seen in the *mutS* gene. The specific mutations identified, their effect on MutS and their abundance in the evolved populations are indicated (mutation detection cut-off = 5%). The last column shows the frequency for each *mutS* mutation over the course of evolution. The X-axis shows the day of adaptation (26 days in Run 1 and 17 in Run 2) and the Y-axis indicates the percentage of the total population that possessed the mutation.

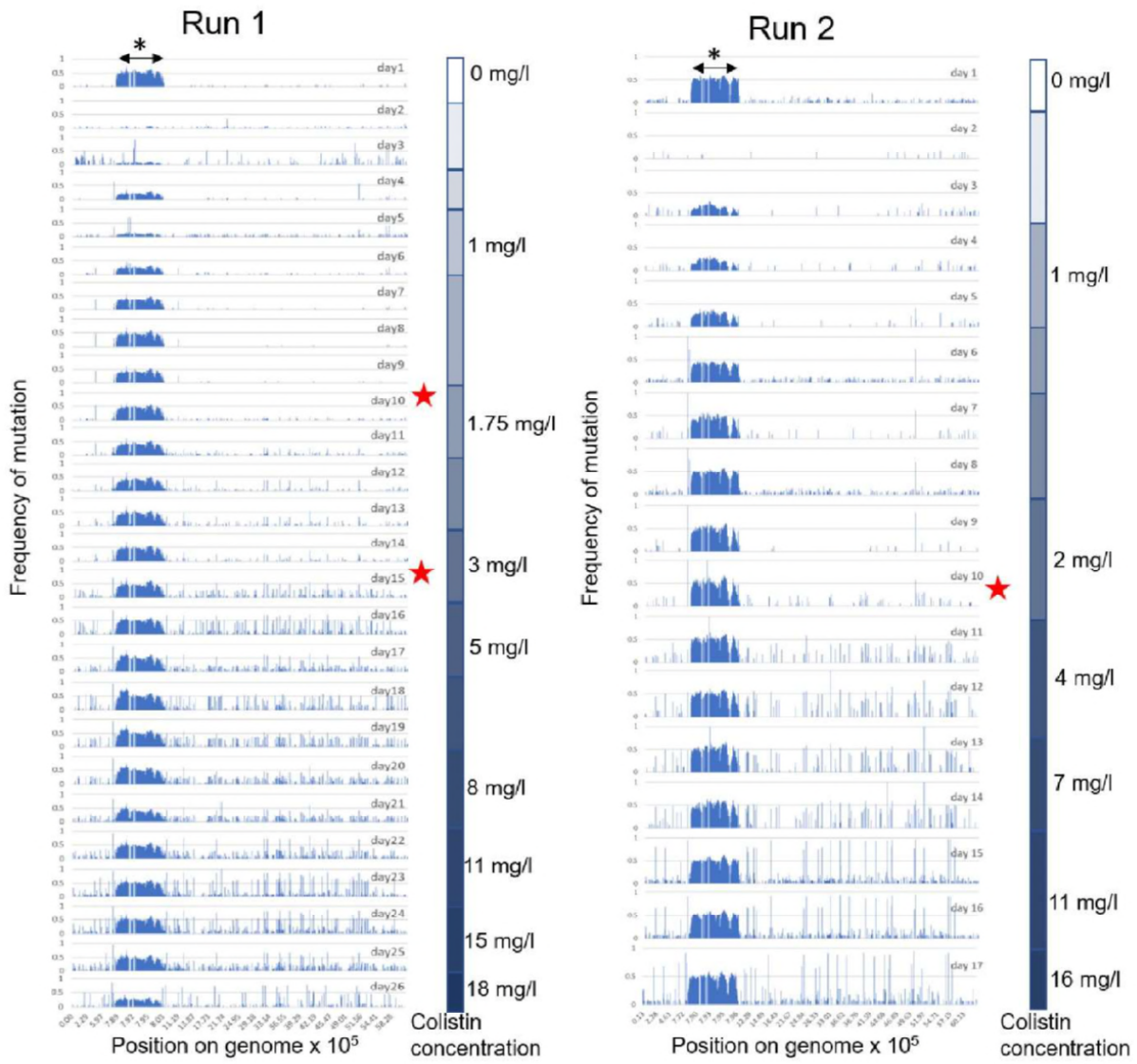

Figure 2. Single nucleotide polymorphism (SNP) map of the PAO1 populations evolving to colistin (Run 1 and Run 2). For ease of comparison, the graphs represent a linearized genome of PAO1 with SNP positions indicated on the X-axis. The X-axis is not distributed evenly but denotes positions on the genome carrying mutations. This is done to highlight regions of the genome with higher mutation density. The Y-axis is the frequency of the mutation in the total population. For each run of adaptation, graphs of daily sampled populations are stacked (26 days of evolution for Run 1 and 17 days for Run 2). Red stars indicate days on which *mutS* mutations

arose in each population. The color gradient on the right side of each panel shows the step-wise increase in colistin concentration experienced by the populations during adaptation. The increased genetic diversity in the region from $7.8x10^5$ to $8x10^5$ bp on the PAO1 genome can be attributed to the Pf4 phage island (indicated by asterisk), details of which are provided in Supplementary file S1.

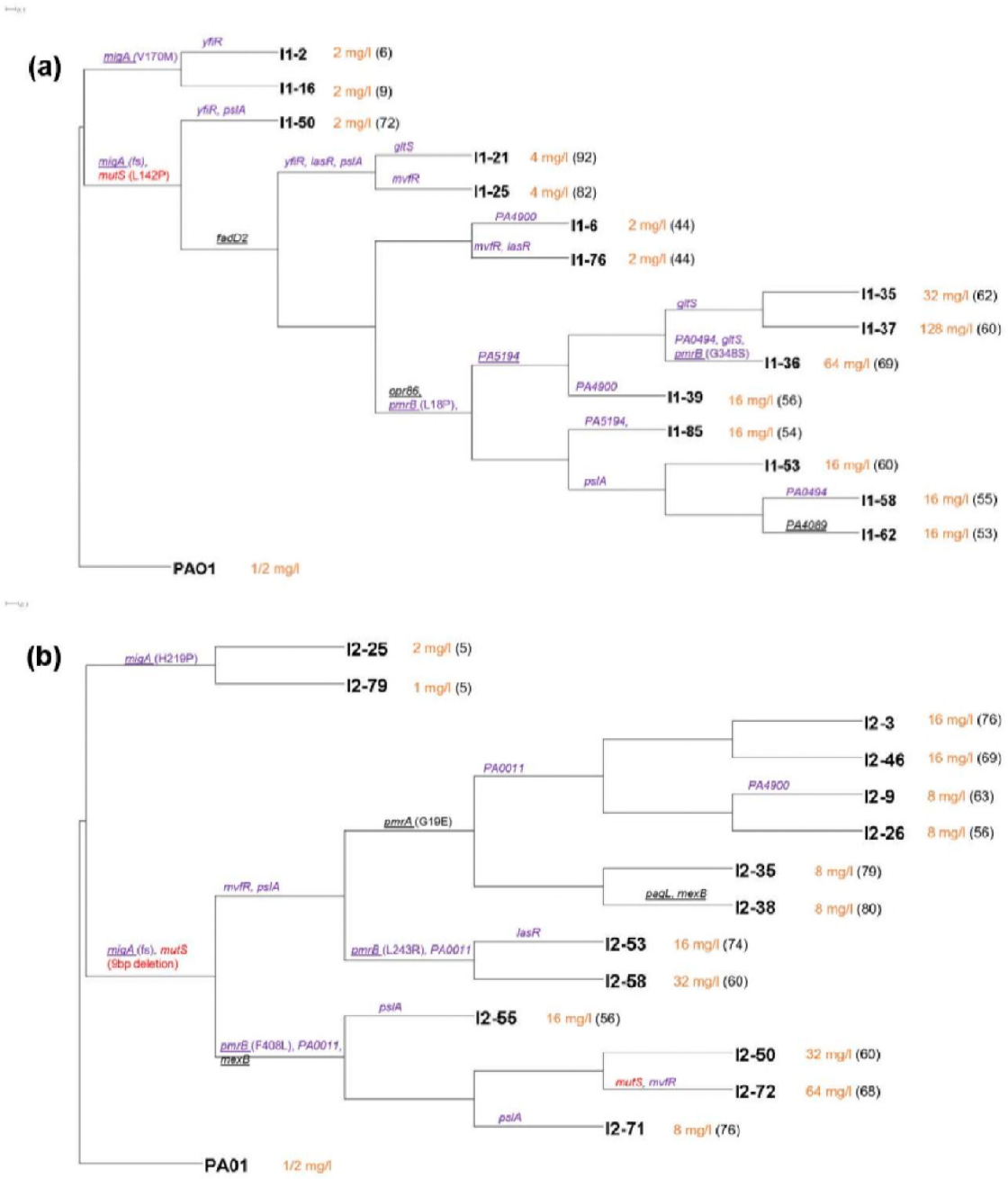

Figure 3. Phylogenetic trees for end point isolates obtained from experimental evolution Runs 1 (a) and 2 (b). PAO1: Ancestor. Isolate names are at the right side of each branch. Orange text following the isolate name denotes its colistin MIC and in parenthesis are the total number of mutations identified in that particular isolate. Branches with mutations in putative targets identified in this study have names of mutated genes on them. Targets in purple text were

identified by the Fisher's Exact test of end point isolates and targets underlined were common among our study and other polymyxin resistance studies. *mutS* mutations are identified in red text. The large number of mutations per hypermutator lineage precludes their complete inclusion in these phylogenetic trees. The complete list of mutations in each end point isolate can be found in Datasets S3 and S4.

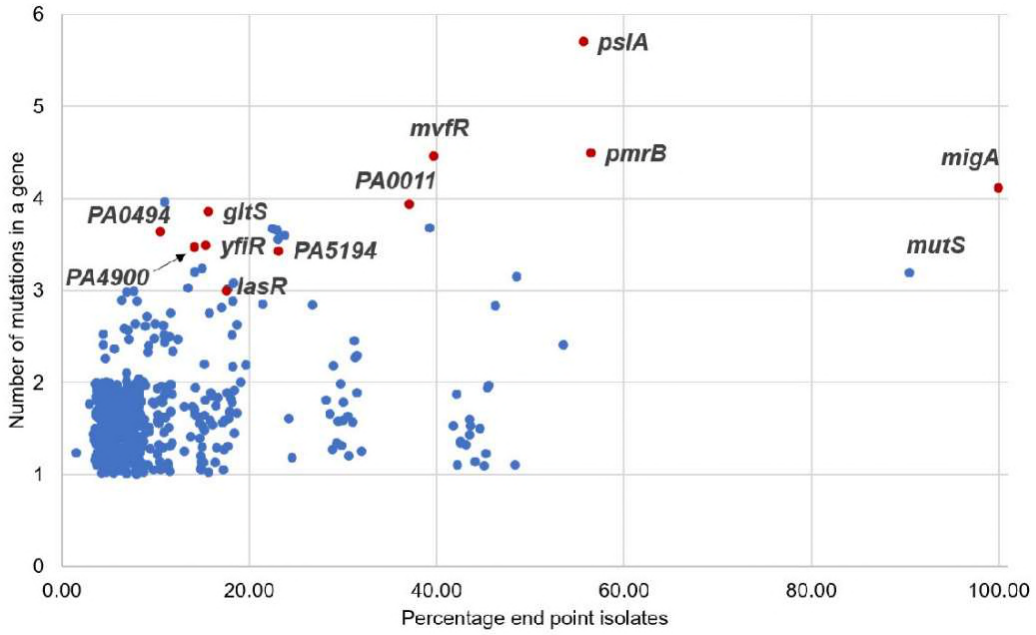

Figure 4. Genes mutated more frequently than expected identified using Fisher's Exact Test. Number of mutations identified within a single gene among the 29 sequenced end point isolates was plotted against the percentage of end point isolates containing a mutation in that gene. Genes identified as significant with a *p* value less than 0.001 in the Fisher's Exact Test are highlighted in red. False noise has been added to the data points to separate them on the graph. Detailed analysis of this graph is provided in Supplementary file S1.

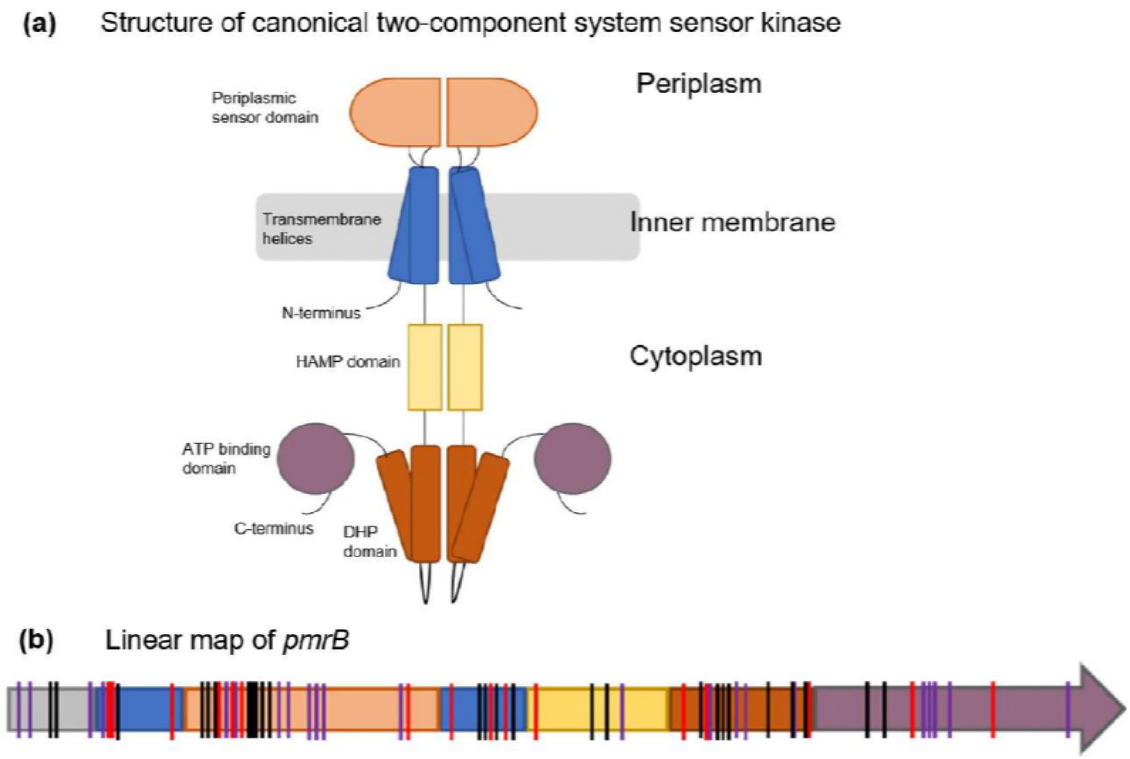

Figure 5: (a) Structural representation of a canonical two-component system sensor kinase dimer (adapted from (38)) and (b) linear map of *pmrB* showing positions of identified mutations. The color scheme for domains used in (a) has been maintained in (b). Mutations identified in *pmrB* in this study as well as previous works have been indicated by vertical lines on the *pmrB* gene (b). Red lines represent mutations identified in this study. Black lines represent mutations observed in other evolution experiments (12, 13, 27, 30) and purple lines represent mutations identified in colistin resistant clinical *P. aeruginosa* isolates (10–12, 26, 35, 36, 39). HAMP: histidine kinases, adenylate cyclases, methyltransferases and phosphodiesterases; DHP: dimerization and histidine phosphotransfer. Domain assignments in the PmrB protein are based on the predicted domain structure of PmrB of Moskowitz et al. (26). Details of the types of mutations observed in each domain of PmrB in this study can be found in Supplementary file S1.

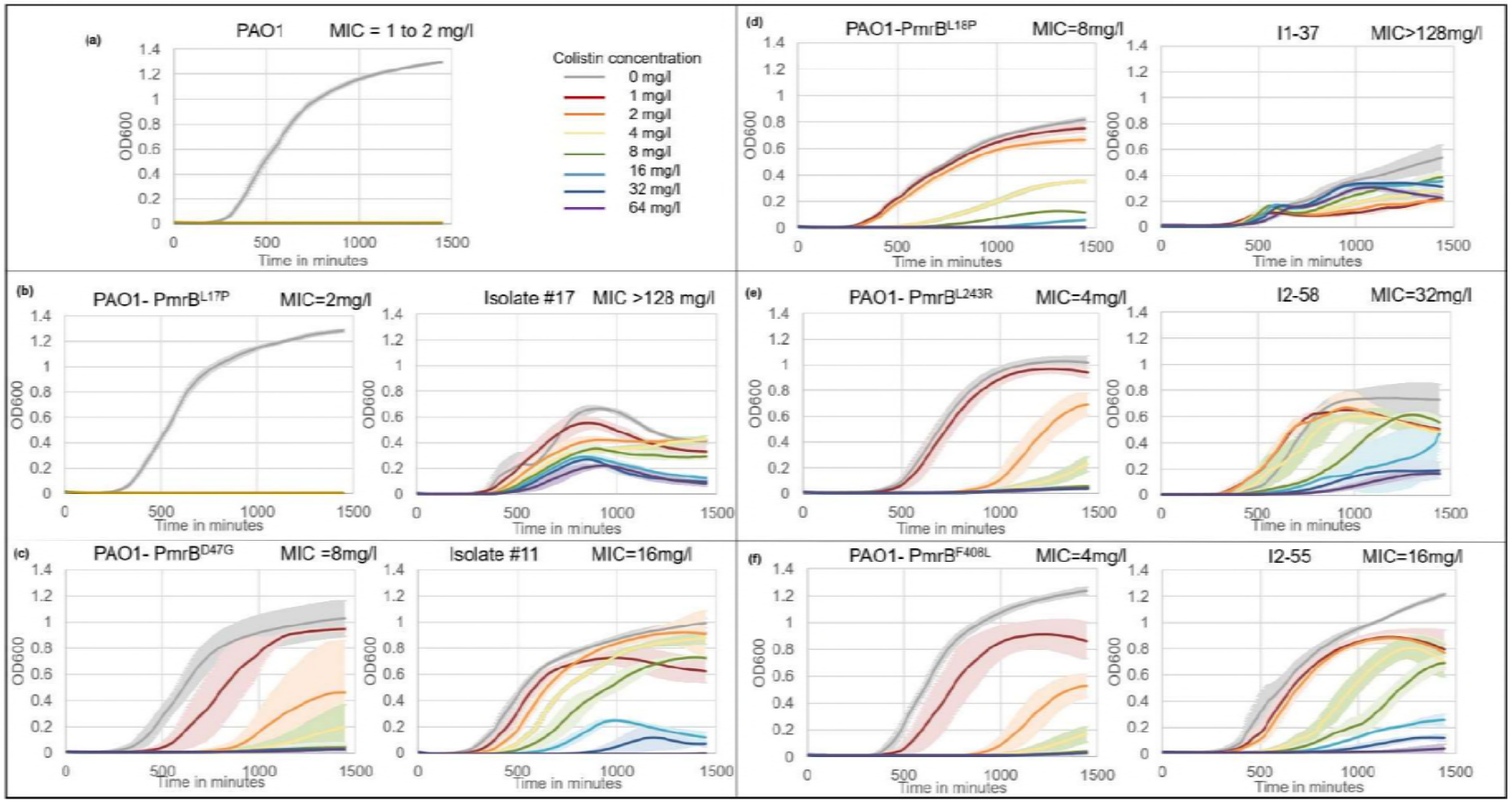

Figure 6. Growth characteristics of PAO1 ancestor, constructed point mutants and bioreactor adapted end point isolates. Each panel (except (a)) represents the constructed mutant on the left and the bioreactor adapted end point isolate carrying the same *pmrB* mutation on the right. All growth assays were conducted at colistin concentrations ranging from 0 to 64 mg/l. Error bars represent the standard deviation of three biological replicates. MICs of all these strains, measured by broth microdilution, are on the top right corner of each graph.

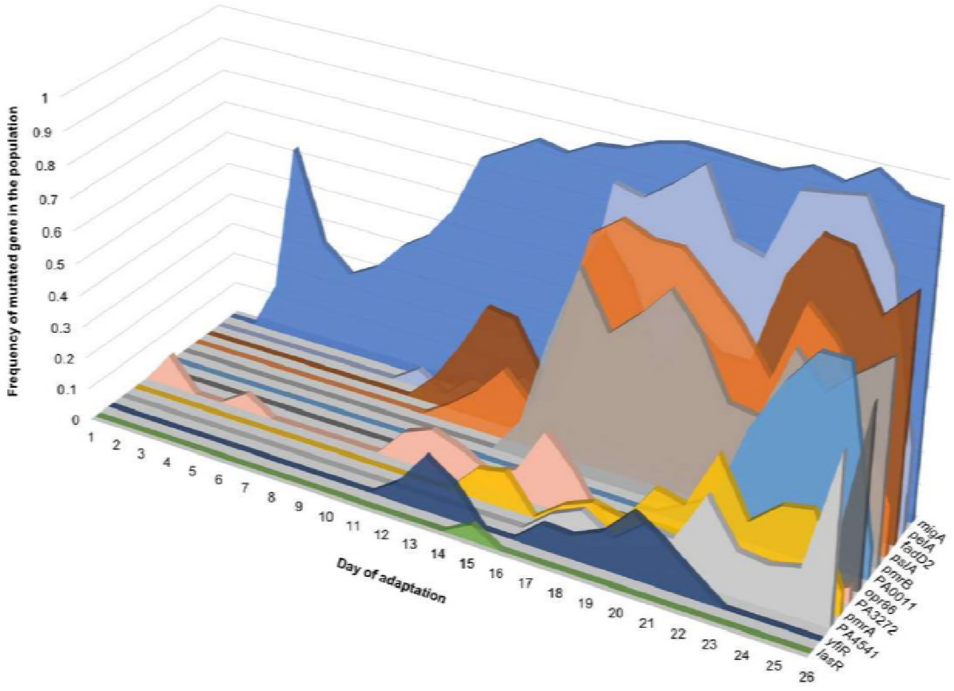

Figure 7: Adaptive genome of a *P. aeruginosa* population (Run 1) evolving to colistin. Most adaptive genes had multiple mutations within them during the course of adaptation. On a given day, the sum of frequencies of the different alleles within a gene was calculated and plotted on the Y-axis. The X-axis represents the day of adaptation and the Z-axis represents each gene. Genes represented here include putative candidates listed in Table 1 and selected candidates from Table 2 (selection based on their appearance in other polymyxin resistance studies).